Simulation and Experiment Research on Liquid Channel of Diffuser Blade by Electrochemical Machining

Jinkai Xu (xujinkai2000@163.com)
Changchun University of Science and Technology
Jin Tao
Changchun University of Science and Technology
Wanfei Ren
Changchun University of Science and Technology
Kun Tian
Changchun University of Science and Technology
Xiaoqing Sun
Changchun University of Science and Technology
Huadong Yu
Changchun University of Science and Technology

Research Article

Keywords: Diffuser blades, ECM, Flow field, Liquid-increasing channel, Uniformity

Posted Date: October 18th, 2021

DOI: https://doi.org/10.21203/rs.3.rs-970521/v1

Version of Record: A version of this preprint was published at The International Journal of Advanced Manufacturing Technology on January 18th, 2022. See the published version at https://doi.org/10.1007/s00170-021-08497-y.

Simulation and experiment research on liquid channel of diffuser blade by electrochemical machining

Jinkai Xu[1] · Jin Tao[1] · Wanfei Ren[1] · Kun Tian[1] · Xiaoqing Sun[1] · Huadong Yu[1]

1 Ministry of Education Key Laboratory for Cross-Scale Micro and Nano Manufacturing, Changchun University of Science and Technology, Changchun 130022, China

Corresponding authors: xujinkai2000@163.com (Jinkai Xu);

renwanfei2020@163.com(Wanfei Ren)

Abstract Aiming to solve the problems of the low electrolyte flow rate at leading edge and trailing edge and poor uniformity of the end clearance flow field during the electrochemical machining (ECM) of diffuser blades, a gap flow field simulation model was established by designing three liquid-increasing channels at the leading edge and the trailing edge of the cathode. The simulation results indicate that the liquid-increasing hole channel (LIHC) with an outlet area S of 1.5 mm^2 and a distance L from channel center to edge point of 3.2 mm achieves optimal performance. In addition, the experiment results show that the optimized cathode with liquid-increasing hole channel (LIHC) significantly improves the machining efficiency, accuracy and surface quality. Specifically, the feed speed increased from 0.25 mm/min to 0.43 mm/min, the taper decreased from 4.02° to 2.45°, the surface roughness value of blade back reduced from 1.146 μm to 0.802 μm. Moreoever, the roughness of blade basin decreased from 0.961 μm to 0.708 μm, and the roughness of hub reduced from 0.179 μm to 0.119 μm. The results prove the effectiveness of the proposed method, and can be used for ECM of other complex structures with poor flow field uniformity.

Keywords Diffuser blades · ECM · Flow field · Liquid-increasing channel · Uniformity

1. Introduction

The diffuser is one of the core components used in the aero engine [1, 2], and its main function is to convert the kinetic energy of high-speed air flow at the impeller outlet

into pressure energy. In order to meet the high performance requirements and adapt to harsh working environments, the diffuser is usually made of titanium alloy or nickel-based superalloy which is resistant to high temperature and corrosion, but has high hardness, low thermal conductivity and is difficult to process. Traditional manufacturing methods will lead to high cutting temperature, low machining surface quality, serious tool wear and high residual stress [3-6]. Electrochemical machining (ECM), however, is a non-traditional machining method based on the anodic electrochemical dissolution mechanism, which is not only suitable for machining difficult-to-cut materials and complex structures, but also has the advantages of no tool wear, no residual stress, high machining efficiency, theoretically no cathode loss and feasible mass manufacturing [7-10]. Therefore, ECM has been widely used in automotive, aerospace, mold industry, medical and other fields [11-13].

In ECM, the distribution of the flow field directly affects the machining stability, machining accuracy and surface quality [14, 15]. In recent years, many researchers have focused their efforts on the flow field of ECM, including ultrasonic assisted ECM to improve the electrolyte flow state in the machining gap [16], and used pulsating electrolyte to improve the surface quality and material removal rate, and employed progressive pressure electrolyte to increase the flow rate in the electrode gap [17,18]. However, the above references have higher requirements for auxiliary external factors. In addition, in the study of flow field mode, in 2013, Xu et al. used Π shape flow mode to ECM the integrated blade cascade channel, and a more uniform flow field improved the processing quality, stability and efficiency [19]. Two years later, the reverse flow field was used to ECM for the closed integral impeller, showing that the whole process was stable, and the machining quality was high [20]. In 2020, Wang et al. designed a new tangential flow field, which effectively eliminated the defect of sudden change of flow channel in ECM for large size blade [21]. In the same year, Liu et al. controlled the flow direction of the electrolyte in the machining area by changing the type of flow channel inside the tool electrode, which can significantly reduce stray corrosion and improve the surface processing quality of TB6 titanium alloy [22]. In 2021, Lei et al. proposed an edge electrolyte supply mode and optimized

the structure of the insulating sleeve, which effectively improved the machining accuracy and machining quality of the overall blade cascade (Ti6Al4V) processed by electrochemical trepanning [23]. Although changing the flow field mode has many advantages, it requires complex tooling. To solve the problems of low electrolyte flow rate at the leading edge and the trailing edge and poor uniformity of the end clearance flow field during ECM of diffuser blades, this work designs three different liquid-increasing channels at the leading edge and the trailing edge of cathode to improve the flow field without external auxiliary conditions and complex tooling. Through flow field simulation, the three liquid-increasing channels were tested and analyzed. By comparison, the LIHC has been proven to promote the end clearance flow field to obtain a better flow state. In order to further improve the uniformity, it is optimized by modifying the structural parameters. Finally, comparative experiments were carried out to verify the effectiveness of the proposed method.

2. Design of flow field mode with liquid-increasing channel

Generally speaking, the flow mode of electrolyte is divided into three categories: side flow, positive flow, and reverse flow [24-26]. In this work, the electrolyte flow is positive flow. In the process of positive flow ECM, the assembled cathode consists of cathode body, insulating layer and cathode piece. The electrolyte is pumped from the top inlet of the cathode, flows through the inner cavity of the cathode body coated with insulating layer, enters the cathode sheet forming groove, and finally flows out from the outer side gap and the end clearance of leading edge and trailing edge, as shown in Fig.1a.

With the continuous feeding of the cathode, the blade of the diffuser is finally processed into a desired shape. However, for electrolyte, a low speed area was observed at the leading edge and the trailing edge in this processing method. This can be understood that the leading edge and the trailing edge witnesses a small diameter but large radian and area, and hence the accessibility of the flow field is low, as shown in Fig.1b. Thus, the low speed leads to non-uniform flow field, which makes the machining unable to continue due to spark short-circuit, thereby causing an uneven

surface of the flow channel and poor processing quality.

In order to solve this problem, three kinds of liquid-increasing channels were designed at the leading edge and the trailing edge of the cathode: liquid-increasing curved seam channel (LICSC), liquid-increasing straight seam channel (LISSC), and liquid-increasing hole channel (LIHC). The inlet of the three kinds of liquid-increasing channels is also at the top of the cathode, passing through the cathode body and cathode piece, and their inlet area is larger than the outlet area, as shown in Fig. 1c, d and e. Therefore, the electrolyte can flow into the end clearance from both the original inlet and the inlet of the liquid-increasing channel at the same time. Thanks to this design, the liquid-increasing channel is on the cathode, which eliminates the complex fixture and tooling, and directly supplies the liquid at the edge. What's more, it shortens the flow distance of the electrolyte, and hence increases the electrolyte flow rate at the edge, improving the accessibility and uniformity of the flow field.

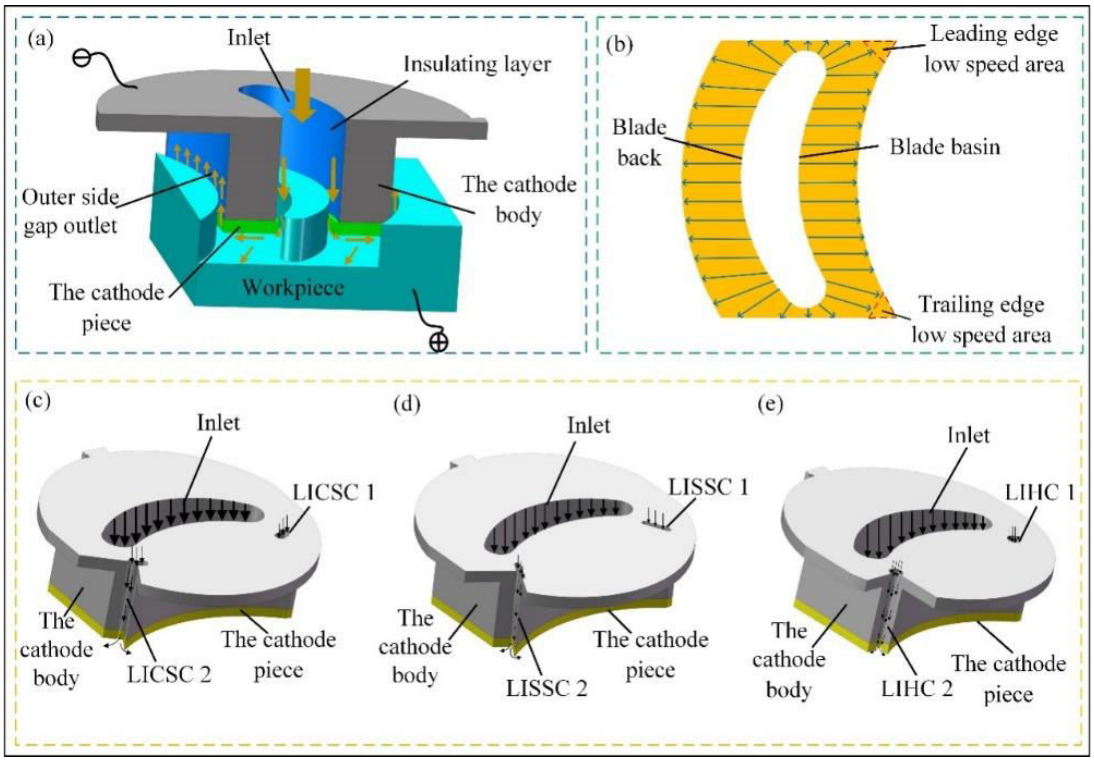

Fig. 1 Schematic diagram of flow field. **a** Positive flow field in ECM. **b** End clearance streamline. **c** Cathode with the LICSC. **d** Cathode with the LISSC. **e** Cathode with the LIHC

3. Simulations

3.1 Establishment of mathematical model

In ECM, the flow field in processing gap is very complex. To simplify the simulation of flow field, the following assumptions were made: (1) the fluid is an incompressible and constant Newtonian fluid, meaning that no matter how the velocity gradient changes, the dynamic viscosity remains unchanged. (2) The influence of bubbles and solid particles in the fluid is not considered, and the bubbles and Joule heat generated during the processing can be ignored. (3) There is no movement and slip at the solid boundary.

The electrolyte is required to be in a turbulent flow state in ECM so as to allow the heat and products generated in the ECM area to be taken away to the greatest extent. The state of laminar flow and turbulent flow is usually distinguished by the Reynolds number *Re*. Therefore, the condition needs to be satisfied to ensure a turbulent flow state:

$$Re = \frac{uD_h}{v} > 2300 \tag{1}$$

$$D_h = \frac{4A}{x} \tag{2}$$

Where u is the flow rate of the electrolyte, D_h is the hydraulic diameter, v is the kinematic viscosity of the electrolyte, A is the area of the flow channel section, x is the wet circumference of the flow channel section.

According to the above assumptions, the motion control equation of the electrolyte in the flow field simulation can adopt the Navier-Stokes equation [27]:

$$\frac{\partial \bar{u}_i}{\partial x_i} = 0 \tag{3}$$

$$\frac{\partial \bar{u}_i}{\partial x_j} + \bar{u}_j \frac{\partial \bar{u}_i}{\partial x_j} = -\frac{\partial \bar{p}}{\partial x_i} + v\frac{\partial^2 \bar{u}_i}{\partial x_j \partial x_j} - \frac{\tau_{ij}}{\partial x_j} \tag{4}$$

where $\bar{u}_i$ represents the component of the time-averaged velocity in the *i* direction, x_i is the coordinate in the *i*-axis direction of the coordinate system, x_j is the same, $\bar{p}$ represents the time-averaged pressure, and τ_{ij} is the component of the stress tensor in the ij plane.

In the internal flow channel of ECM of diffuser blades, the channel shape is complex and the electrolyte streamline is curved. Therefore, the RNG *k*-*ε* flow model suitable for the flow on the curved wall was selected to solve the simulation of three-dimensional ECM gap flow field [28, 29]. The turbulent kinetic energy k and the dissipation rate equations ε are as follows:

$$\frac{\partial \rho k}{\partial t}+\frac{\partial\left(\rho k u_i\right)}{\partial x_i}=\frac{\partial}{\partial x_j}\left[\left(\mu+\frac{\mu_t}{\sigma_k}\right)\frac{\partial k}{\partial x_j}\right]+G_k-\rho\varepsilon \tag{5}$$

$$\frac{\partial(\rho\varepsilon)}{\partial t}+\frac{\partial\left(\rho\varepsilon u_i\right)}{\partial x_i}=\frac{\partial}{\partial x_j}\left[\left(\mu+\frac{\mu_t}{\sigma_\varepsilon}\right)\frac{\partial \varepsilon}{\partial x_j}\right]+\frac{C_1\varepsilon}{k}G_k-C_2\rho\frac{\varepsilon^2}{k} \tag{6}$$

$$\mu_t=\rho C_\mu k^2/\varepsilon \tag{7}$$

where G_k is the turbulent kinetic energy generation term caused by the average velocity gradient, μ is the viscosity coefficient, ρ is the density of the electrolyte, μ_t is the turbulent viscosity, t is the time, x_i and x_j are coordinate positions, u_i is the velocity in the x_i direction, $C_1, C_2, C_\mu, \sigma_\varepsilon, \sigma_k$ is the model constant, C_1=1.44, C_2 =1.92, C_μ=0.09, σ_ε=1.3, σ_k=1.1.

3.2 Three dimensional flow field model and boundary conditions

According to the actual processing conditions, the original model (Fig. 2a), the LICSC model (Fig. 2c), the LISSC model (Fig. 2d), and the LIHC model (Fig. 2e) were established in the SolidWorks software. Fig. 2b is the cross-sectional view of plane B. The above four models were selected when the machining depth *h* was 5 mm, the end clearance Δb_1 and the outer side gap Δb_2 were both set to 0.5 mm, the inlet area and outlet area of the three liquid-increasing channels were the same. In the simulation process, the original inlet and the inlet of the LICSC, the inlet of the LISSC, and the inlet of the LIHC had the same pressure of 0.73 MPa, while the outlet pressure was set as 0 MPa.

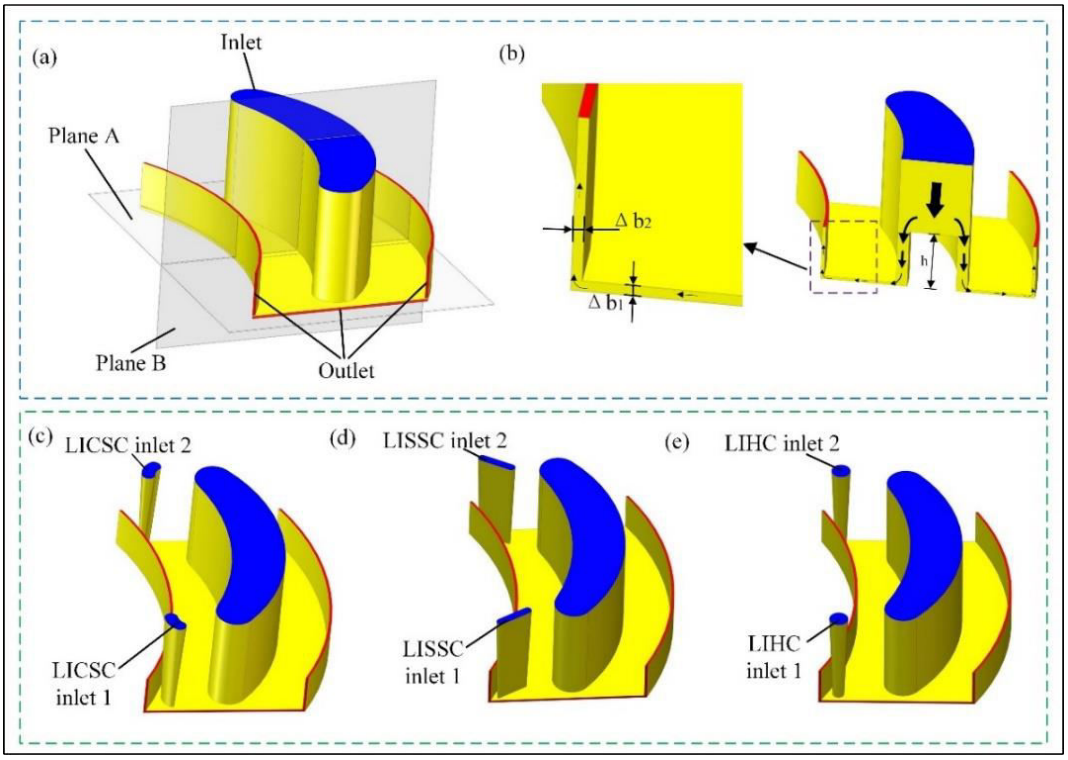

Fig. 2 Three-dimensional flow field model. **a** The original model. **b** The cross-sectional view of plane B. **c** The LICSC model. **d** The LISSC model. **e** The LIHC model.

3.3 Flow field simulation and analysis

FLUENT software was used to simulate the flow field of the original model, the LICSC model, the LISSC model, and the LIHC model. The section A in the middle of the end clearance was selected as the reference section of the processing area, and the effects of the three liquid-increasing channels on the velocity distribution of electrolyte in the ECM of diffuser blades were compared. Fig. 3 shows the velocity distribution on section A of four different models. It can be seen from the velocity cloud diagram that in the original model flow field (Fig. 3a), the electrolyte flow rate was low at the leading edge and the trailing edge, the anode dissolved product could not be quickly taken away during processing, and hence the uniformity of the flow field was poor, resulting in an unstable machining and even short circuits. By contrast, in the flow field of three liquid-increasing channels, the electrolyte velocity at the leading edge and the trailing edge was improved, and the overall flow field distribution was more uniform (Fig. 3b, c, d).

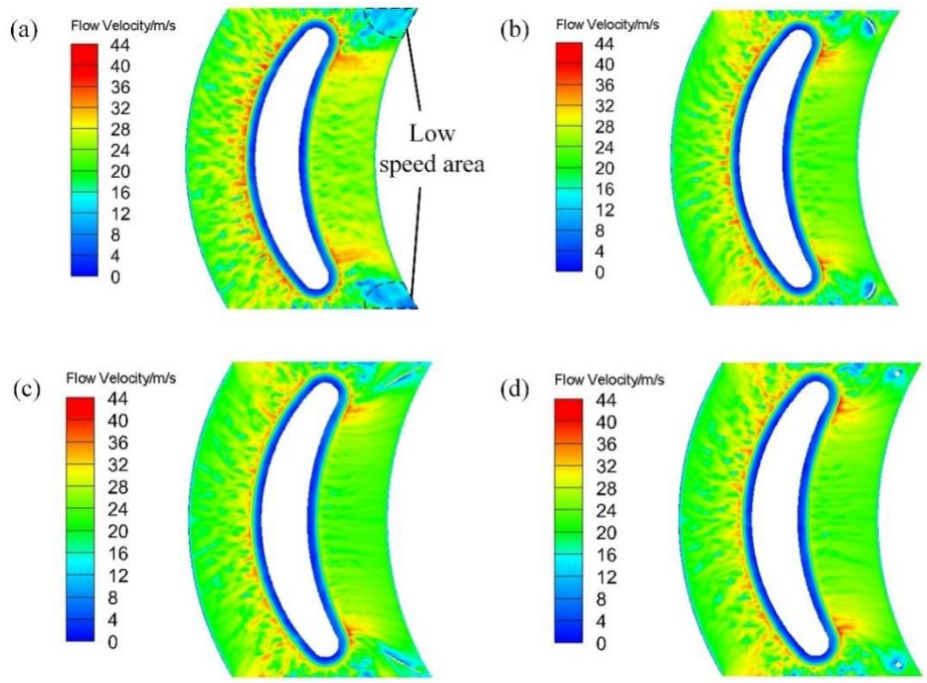

Fig. 3 Velocity cloud diagram of section A. **a** The original model. **b** The LICSC model. **c** The LISSC model. **d** The LIHC model

In order to understand the flow velocity at the edge and the uniformity of the flow field of the entire section more intuitively, 12,569 points were uniformly extracted at each of the two edges, and 182,473 points were evenly extracted across the entire section. Their velocities were obtained in post-processing step. The average flow velocities at the leading edge and the trailing edge were set to u_{a1} and u_{a2}, and the variance of the flow velocity across the section A was set to σ_u, and the results are shown in Table 1. According to Fig. 3 and Table 1, compared with the flow field of the LICSC and the LISSC, the flow velocity at the edge of the LIHC flow field was faster, the overall variance was smaller, and the velocity distribution was more uniform. This may be because the shape of the LIHC is more sufficient for the low speed area and can be better integrated with the original inlet electrolyte. Under the same inlet area and inlet pressure, it can be seen from Eq. (1) that the hydraulic diameter of the LIHC and the Reynolds number are larger, so the electrolyte is less affected by viscous force.

Table 1 Evaluation index values under different modles

Flow field structure	u_{a1}	u_{a2}	σ_u
Original model	12.25	13.51	38.30
LICSC model	17.57	17.90	34.68
LISSC model	17.73	17.58	34.59
LIHC model	18.20	18.50	32.86

3.4 Optimization of the LIHC

Under the condition of flow field with the LIHC, the uniformity of the flow field can be effectively controlled by adjusting the outlet area and the position of the LIHC. Next, therefore, the above two influencing factors were optimized.

3.4.1 Optimization of outlet area of the LIHC

Due to the limitation of cathode structure, the inlet area of the LIHC was fixed at 4.2 mm^2, and then the outlet area S was set to 0.9 mm^2, 1.1 mm^2, 1.3 mm^2, 1.5 mm^2 and 1.7 mm^2, respectivley. The velocity cloud diagrams under each outlet area were obtained, as shown in Fig. 4.

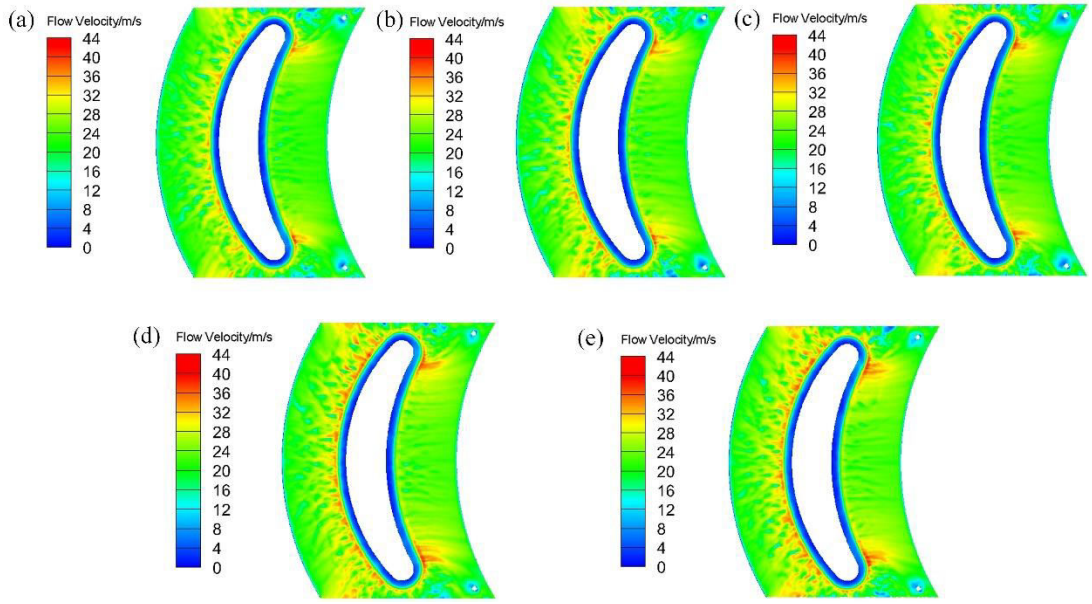

Fig. 4 Velocity cloud diagram for different outlet areas S. **a** 0.9 mm^2. **b** 1.1 mm^2. **c** 1.3 mm^2. **d** 1.5 mm^2. **e** 1.7 mm^2

The same number of points as above were extracted at the leading edge (region

1), at the trailing edge (region 2) and the whole section A through the velocity distribution cloud diagram, and the u_{a1}, u_{a2}, σ_u under different outlet areas S are shown in the Fig. 5. It is seen that the electrolyte supply of the LIHC with small outlet area to the large low speed area was insufficient, and the electrolyte flow rate of the LIHC with the large outlet area failed to meet the requirements. When the outlet area S was 1.5 mm^2, the electrolyte flow rate in region 1 and region 2 reached the highest and the overall variance was the lowest (18.64 m/s, 18.62 m/s and 32.52 m^2/s^2 respectively). Therefore, 1.5 mm^2 was considered to be the optimal outlet area of the LIHC.

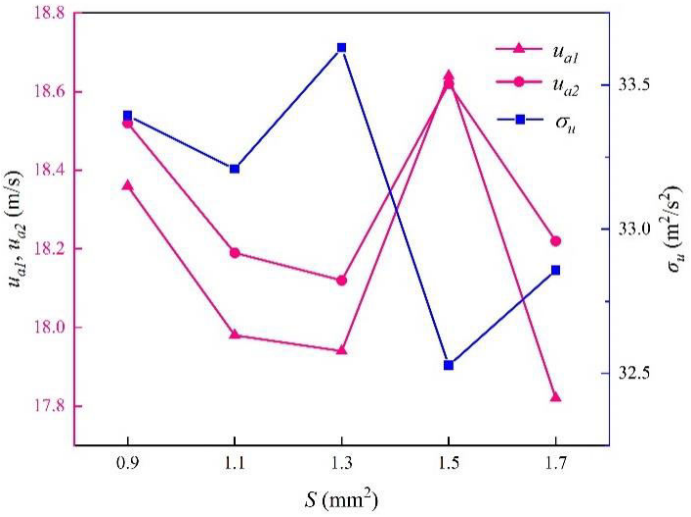

Fig. 5 u_{a1}, u_{a2} and σ_u under different S values

3.4.2 Optimization of the position of the LIHC

The center point of the LIHC is located on the line connecting the edge point with the intersection of the blade basin and the leading edge and the trailing edge. The distance L between the edge point and the center point of the LIHC (Fig. 6a) directly affects the electrolyte flow in the edge area, so six flow models were established based on different distances: 2.3 mm, 2.6 mm, 2.9 mm, 3.2 mm, 3.5 mm and 3.8 mm. Fig. 6b shows the simulation results under different L values. It can be seen from the figure that the increasing distance L caused the electrolyte flow rates u_{a1} and u_{a2} in the two edge areas to first increase and then decrease. When L was 3.2 mm, u_{a1} and u_{a2} reached their maximum values of 19.15 m/s and 19.29 m/s respectively, and σ_u was 31.47 m^2/s^2, the minimum. As a matter of fact, if L was small, the electrolyte supply of the LIHC to the low speed area was uneven. On the other hand, if L was large, the

LIHC would have a great influence on the original inlet flow field. Therefore, the distance L was selected to be 3.2 mm.

By optimizing the outlet area and position of the LIHC, the optimal parameters were obtained: the outlet area S was 1.5 mm^2 and the distance L between the edge point and the center point of the LIHC was 3.2 mm. This optimized LIHC can effectively increase the electrolyte flow rate at the edge and improve the uniformity of the flow field in the processing area.

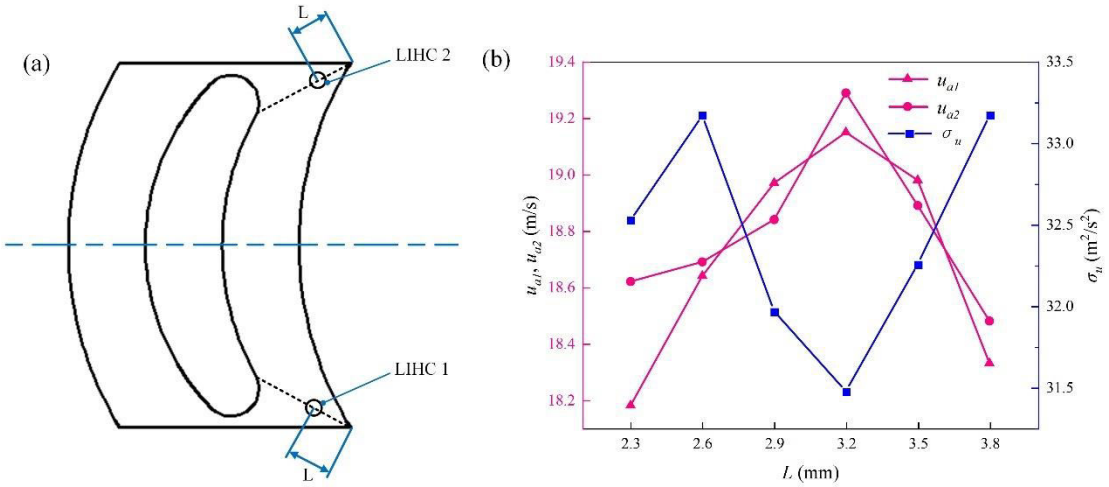

Fig. 6 a Schematic diagram of distance L. **b** u_{a1}, u_{a2} and σ_u under different L values

4. Experiment and discussion

For the purpose of verifying the effectiveness of flow field simulation, the original cathode without the LIHC and an optimized cathode with the LIHC having the outlet area S of 1.5 mm^2 and the distance L of 3.2 mm (Fig. 7b) were fabricated. The material of the cathode body was stainless steel, and the material of the cathode piece was red copper. The comparative experiment was conducted on the ECM equipment (PECM, 800S, Germany).The experimental setup is shown in the Fig. 7a. For analyzing the effect of the LIHC, the analysis was carried out from three aspects: machining efficiency, taper angle and surface roughness. The experimental conditions are shown in Table 2. The voltage was set to 20 V because it is more suitable for processing nickel-based superalloy materials. The inlet pressure was the same as the simulation value, and the machining depth was equal to the axial height of the diffuser blade.

Table 2 ECM experiment conditions

Conditions	Values
Workpiece material	Nickel-based superalloy K418
Electrolyte	20 % $NaNO_3$
Electrolyte temperature	30˚C
Voltage	20V
Inlet pressure	0.73MPa
Machining depth	8.5mm

4.1 Machining efficiency analysis

The feed rate was introduced in the comparative experiment to study the influence of the LIHC on the machining efficiency. Under the condition of using the original cathode and the feed rate of 0.25 mm/min (Fig. 7c), the whole machining process was relatively stable without short circuit, but the current fluctuation was large and there were slight ablative marks at the edge. The surface morphology of the hub at the leading edge and the trailing edge was observed by scanning electron microscope(ZEISS, EVO 20, Germany). Due to the poor uniformity of the flow field in the end clearance, the electrolyte flowed divergently, and obvious flow marks were observed on the hub at the leading edge and the trailing edge. When the feed speed of the original cathode was increased to 0.3 mm/min (Fig. 7d), the actual feed depth of the cathode was 1.2 mm, there were severe ablation marks at the edge, resulting in short circuit during the process. In contrast, when the optimized cathode was used and the feed speed was 0.43 mm/min (Fig. 7e), the current fluctuation was small, no short circuit occurred in the whole machining process, the hub surface was very smooth, and there was no obvious flow marks at the leading edge and the trailing edge. The results show that the optimized cathode can effectively improve the machining efficiency.

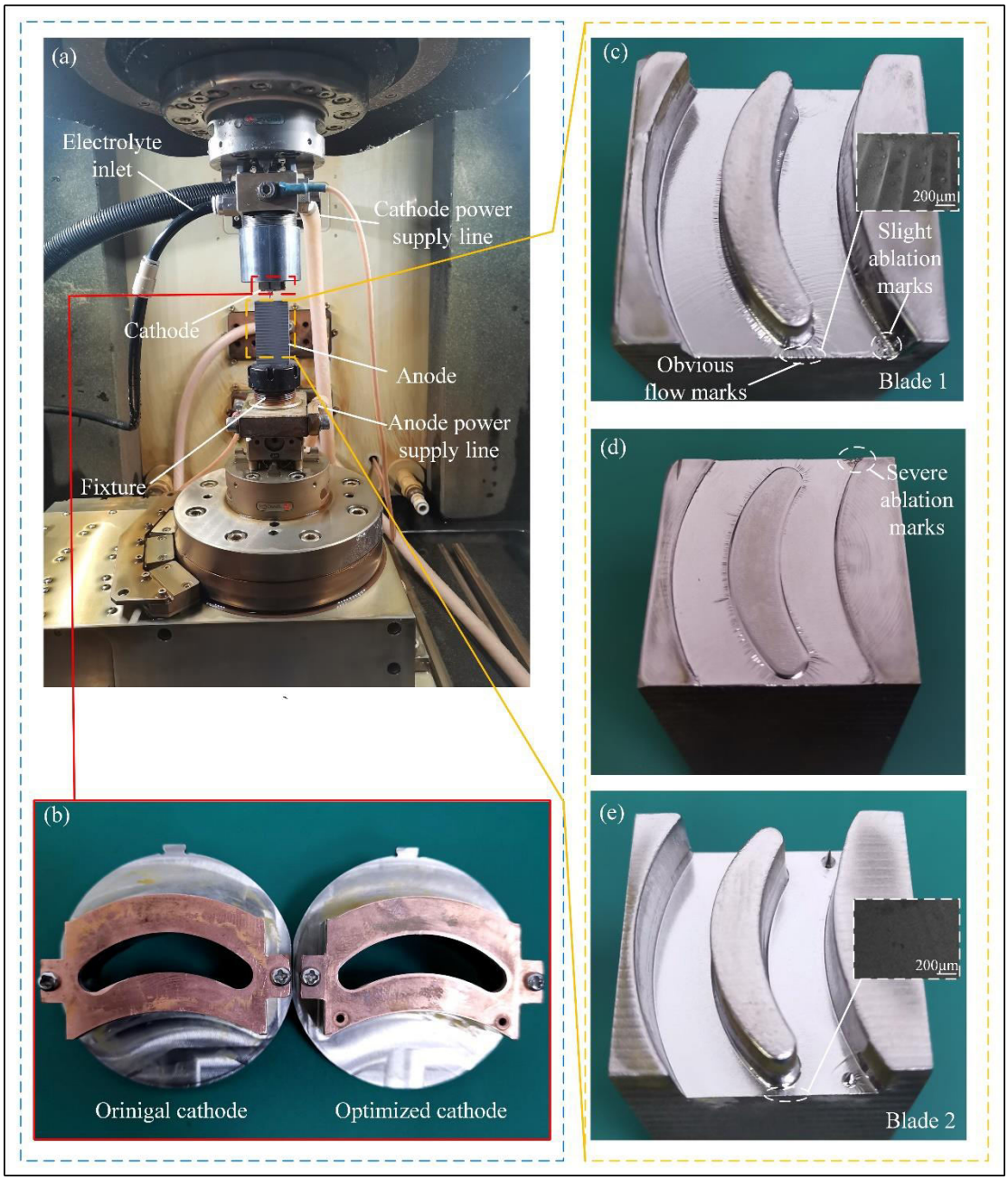

Fig. 7 a Experiment setup of ECM. **b** Experimental cathodes. **c** The machined blade by original cathode at a feed rate of 0.25 mm/min. **d** The machined blade by original cathode at a feed rate of 0.3 mm/min. **d** The machined blade by optimized cathode at a feed rate of 0.43 mm/min

4.2 Taper analysis

Blade 1 was machined with the original cathode at a feed rate of 0.25 mm/min, while, blade 2 was processed using the optimized cathode at a feed rate of 0.43 mm/min. To measure the machining accuracy of the two groups of blades, three sections were selected at the leading edge, the trailing edge and the middle position of the two groups of machined blades. A three-dimensional optical microscope (Zeiss-Smart

Zoom 5, Germany) was used to measure the profile of each section. The leading edge sections of blade 1 and blade 2 are shown in Fig. 9a, b. The taper angle α (Fig. 8) was calculated according to the formula, which was defined as:

$$\alpha = \arctan\left(\Delta L / H\right) \tag{8}$$

$$\Delta L = \left(L_2 - L_1\right) / 2 \tag{9}$$

where L_1 is the transverse distance of blade tip, L_2 is the transverse distance of blade root, ΔL is the transverse distance error between blade root and blade tip on one side of blade, H is the height of the machined blade.

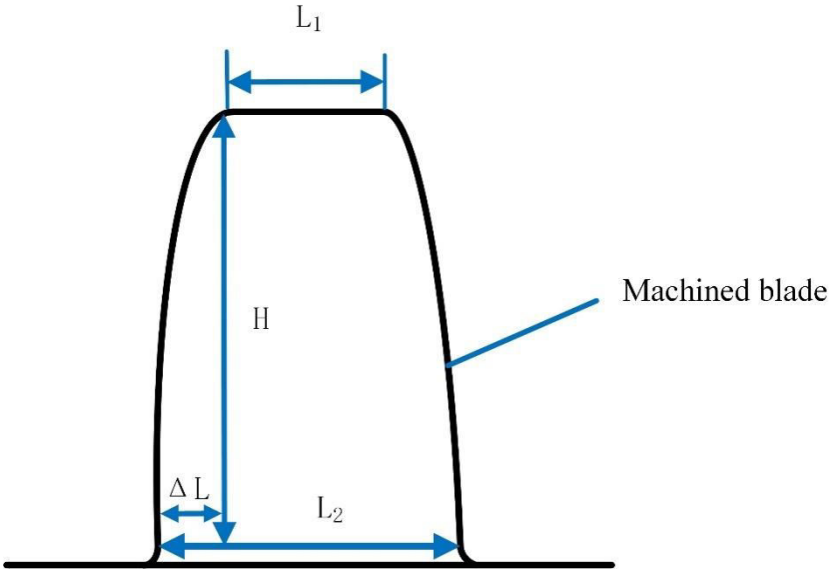

Fig. 8 Schematic diagram of the blade taper of the diffuser

The taper angle measurement results are shown in Fig. 9. The comparative results of the two groups of blades illustrated that the taper angle of the leading edge decreased from 5.16° to 2.42°, the taper angle of the middle position decreased from 3.61° to 2.59°, the taper angle of the trailing edge decreased from 3.29° to 2.34°, and the average taper angle of the three sections decreased from 4.02° to 2.45°, which indicated that the taper angle was significantly reduced. This can be explained by the fast feed speed. Specifically, the fast feed rate causes the blade to leave the cathode edge and enter the cathode body with an insulating layer in a fast manner, and hence the time of stray corrosion caused by the residual current on the cathode edge was short. In addition, the machining gap becomes smaller due to the fast rate, which is conducive to improving the machining accuracy. Besides, it can be seen from the

taper angles of the three sections that the uniform flow field in the process of machining blade 2 could make the machining allowance more consistent.

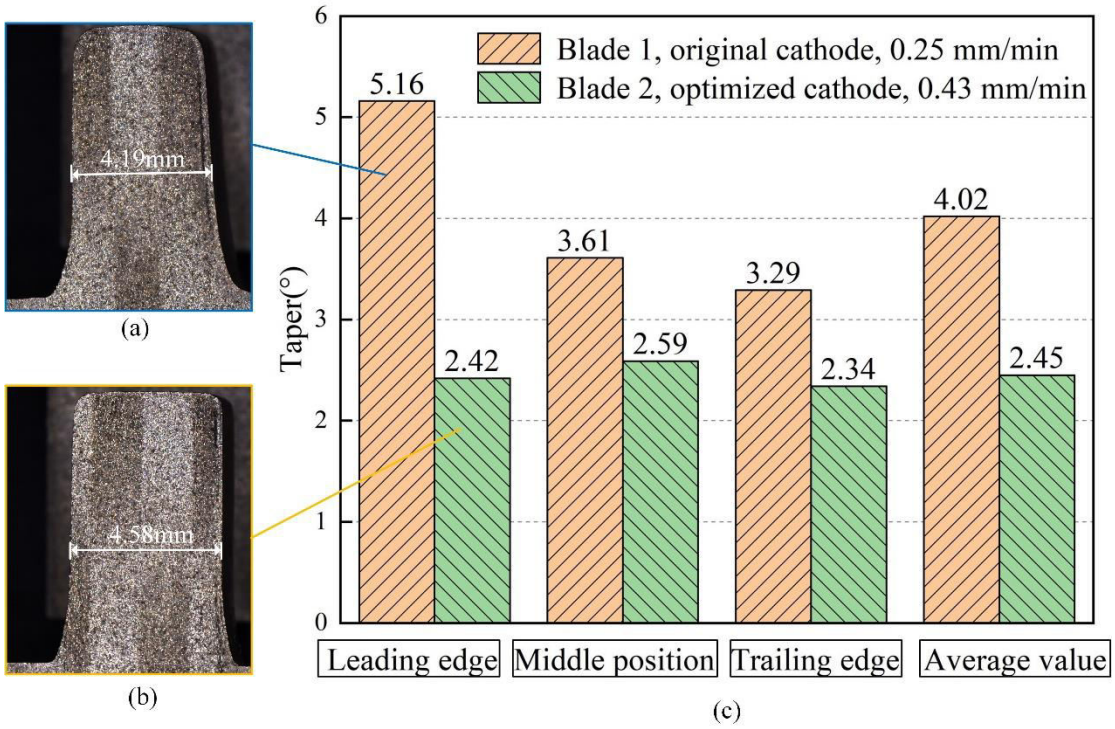

Fig. 9 a The leading edge sections of blade 1. **b** The leading edge sections of blade 2. **c** Measurement results of blade taper angles

4.3 Surface roughness analysis

The surface roughness of the machined blades was obtained by using a surface profilometer (Mahr, MarsurfLD 120, Germany). To ensure the measurement accuracy, five measurement lines were evenly selected on the blade basin surface, blade back surface and hub surface of blade 1 and blade 2 respectively. The average results of the five measurement lines are listed in the Fig. 10a. It can be seen that the surface roughness of blade back was reduced from 1.146 μm to 0.802 μm, the surface roughness of blade basin was reduced from 0.961 μm to 0.708 μm, and the surface roughness of the hub was reduced from 0.179 μm to 0.119 μm. The surface quality of blade 2 was better than that of blade 1. This is because fabricating LIHC helps accelerate the flow rate of electrolyte at the edge, and hence the uniformity of the flow field was improved, which causes the electrolytic products and bubbles affecting the surface roughness to be quickly taken away. On the other hand, due to the faster feed speed and smaller processing area, the current density becomes larger and the

workpiece dissolves evenly, resulting in a significantly reduced surface roughness.

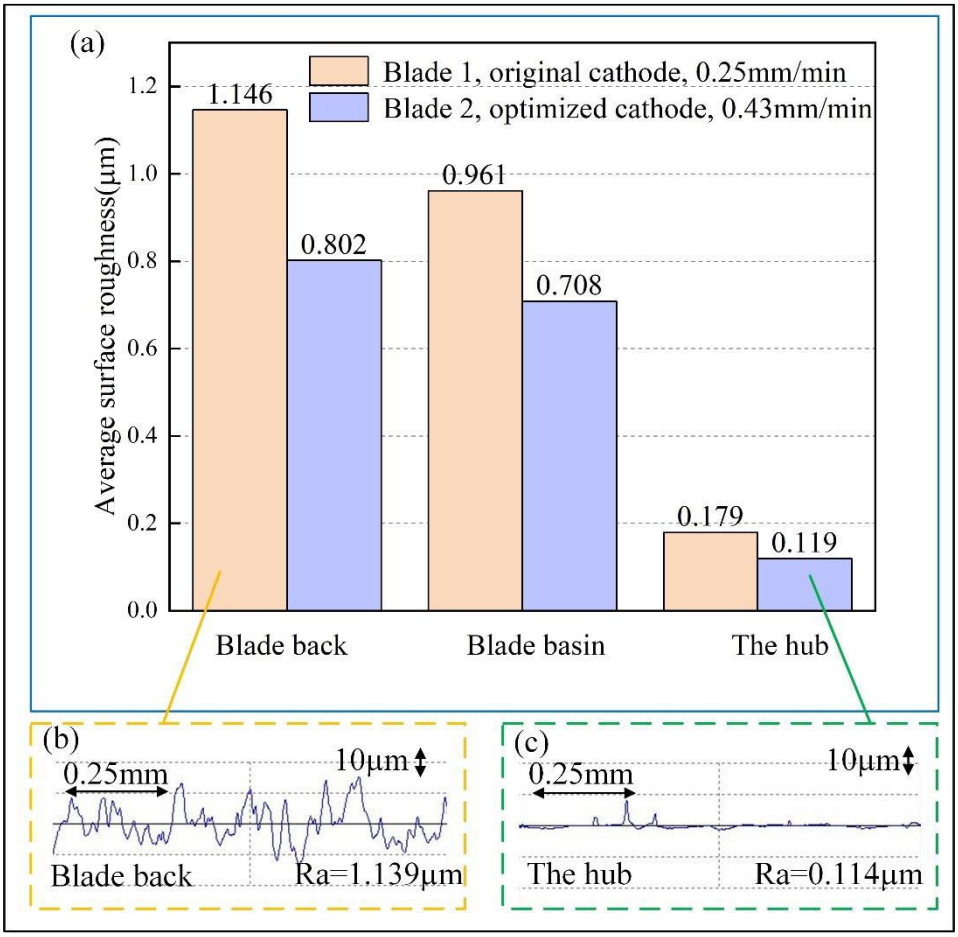

Fig. 10 Surface roughness measurement results. **a** Average surface roughness. **b** Blade back surface roughness measuring line 1 of blade 1. **c** The hub surface roughness measuring line 1 of blade 2

5. Conclusions

In this paper, a method of liquid-increasing channel was proposed to improve the uniformity of flow field in ECM, and the conclusions can be drawn as follows:

(1) Three kinds of liquid-increasing channels for direct liquid supply were designed at the leading edge and the trailing edge of the cathode, which improves the flow field distribution of the end clearance and eliminates the complex fixture and tooling.

(2) According to different structures of the liquid-increasing channel, the corresponding flow field model was established and the flow field simulation was carried out. The results show that the LIHC achieves the best improvement effect on the flow field of the end clearance. The electrolyte velocity at the leading edge and the

trailing edge was increased, and the flow field uniformity of the end clearance was improved.

(3) The optimal design of the LIHC was carried out, and the optimal parameters were obtained. The optimal values of the outlet area *S* and the distance between the center of the LIHC and the edge point *L* were 1.5 mm^2 and 3.2 mm respectively.

(4) The comparative experiments show that the optimized cathode with the LIHC increased the feed rate from 0.25 mm/min to 0.43 mm/min, and the taper decreased from 4.02˚ to 2.45˚. Besides, the surface roughness value of blade back was reduced from 1.146 μm to 0.802 μm, the value of blade basin decreased from 0.961 μm to 0.708 μm, and the value of hub reduced from 0.179 μm to 0.119 μm. This method can be applied to ECM other complex structures with low speed flow field, creating social and economic value in engineering applications.

Author contribution Jinkai Xu and Wanfei Ren was responsible for substantive revision; Jin Tao drafted the manuscript and performed the experiments; Kun Tian assisted in the experiment; Xiaoqing Sun performed the interpretation of data; Huadong Yu contributed to the design of the work.

Funding This work was supported by National Natural Science Foundation of China (U19A20103); The Fund for Jilin Province Scientific and Technological Development Program (No. Z20190101005JH); The Fund for The Central Government Guides Local Science and Technology Development Funds to the special basic research of Jilin Province (No. 202002039JC).

Availability of data and materials We confirm that the data and materials supporting the findings of this study are available within the article.

Declarations

Ethical approval Not applicable.

Code availability Not applicable.

Consent to participate Not applicable.

Consent to publish Not applicable.

Competing interests The authors declare no competing interests.

References

[1] Benichou E, Trebinjac I (2016) Comparison of steady and unsteady flows in a transonic radial vaned diffuser. J Turbomach. 138(12):121002-1-10

[2] Marsan A, Trébinjac I, Coste S, Leroy G (2013) Temporal behaviour of a corner separation in a radial vaned diffuser of a centrifugal compressor operating near surge. J Therm Sci 22(6):555–64

[3] González-Barrio H, Calleja-Ochoa A, Lamikiz A, López de Lacalle LN (2020) Manufacturing Processes of Integral Blade Rotors for Turbomachinery, Processes and New Approaches. Applied Sciences 10(9):3063

[4] Klocke F, Zeis M, Klink A, V eselovac D (2012) Technological and economical comparison of roughing strategies via milling, EDM and ECM for titanium- and nickel-based blisks. Proc CIRP 2:98–101

[5] Musfirah H, Ghani A, Haron C (2017) Tool wear and surface integrity of inconel 718 in dry and cryogenic coolant at high cutting speed. Wear 376-377:125-133

[6] Xu JK, Ren WF, Lian ZX, Yu P, Yu HD (2020) A review: development of the maskless localized electrochemical deposition technology. Int J Mach Tools Manuf 110(2)

[7] Klocke F, Zeis M, Klink A, V eselovac D (2013) Experimental research on the electrochemical machining of modern titanium- and nickel-based alloys for aero engine components. Procedia CIRP 6:368–372

[8] Davydov D, Kabanova B, Volgin M (2017) Electrochemical machining of titanium. Review. Russian Journal of Electrochemistry 53(9):941-965

[9] Lohrengel M M, Rataj K P, T Münninghoff (2016) Electrochemical Machining-mechanisms of anodic dissolution. Electrochimica Acta 201:348-353

[10] Holstein N, Krauss W, Konys J (2011) Development of novel tungsten processing technologies for electrochemical machining (ECM) of plasma facing components. Fusion Eng Des 86(9–11):1611–1615

[11] Liu GX, Zhang YJ, Natsu W (2019) Influence of electrolyte flow mode on characteristics of electrochemical machining with electrolyte suction tool. Int J Mach Tools Manuf 142:66-75

[12] Rajurkar KP, Sundaram MM, Malshe AP (2013) Review of electrochemical and electrodischarge machining. Procedia CIRP 6:13–26

[13] Burger M, Koll L, Werner EA, Platz A (2012) Electrochemical machining characteristics and resulting surface quality of the nickel-base single-crystalline material LEK94. J Manuf Process 14(1):62–70

[14] McGeough JA (1974) Principles of electrochemical machining. Chapman and Hall, London

[15] Deconinck D, Van Damme S, Albu C, Hotous L, Deconinck J (2011) Study of the effects of heat removal on

the copying accuracy of the electrochemical machining process. Electrochim Acta 56(16):5642–5649

[16] Sebastian S (2011) Research on ultrasonically assisted electrochemical machining process. Int J Adv Manuf Technol 52:565–574

[17] Qu NS, Fang XL, Zhang YD, Zhu D (2013) Enhancement of surface roughness in electrochemical machining of Ti6Al4V by pulsating electrolyte. Int J Adv Manuf Technol 69(9–12):2703–2709

[18] Qu NS, Hu Y, Zhu D, Xu ZY (2014) Electrochemical machining of blisk channels with progressive pressure electrolyte flow. Mater Manuf Processes 29:572–578

[19] Xu ZY, Sun LY, Hu Y, Zhang JC (2013) Flow field design and experimental investigation of electrochemical machining on blisk cascade passage. Int J Adv Manuf Technol 71(1-4):459-469

[20] Tang L, Yang F, Zhu QL, Gan WM (2015) Electrochemical machining flow field simulation and experimental verification for irregular vortex paths of a closed integer impeller. Int J Adv Manuf Technol 83(1-4):275-283

[21] Wang Y, Xu Z, Liu J, Zhang A, Xu ZL, Meng DM, Zhao JB (2020) Study on flow field of electrochemical machining for large size blade. International Journal of Mechanical Sciences 190:106018

[22] Liu Y, Qu NS (2020) Improvements to machining surface quality by controlling the flow direction of electrolyte during electrochemical sinking and milling of titanium alloy. Science China(Technological Sciences) v.63(12):234-244

[23] Lei GP, Zhu D, Li JB (2021) Optimization of flow field in electrochemical trepanning of integral cascades (Ti6Al4V). Chinese Journal of Aeronautics

[24] Zhu D, Gu ZZ, Xue TY, Liu A (2017) Simulation and experimental investigation on a dynamic lateral flow mode in trepanning electrochemical machining. Chinese Journal of Aeronautics 30(4):1624-1630

[25] Xu JW, Zhu D, Lin JH, Hu XY (2020) Flow field design and experimental investigation of electrochemical trepanning of diffuser with a special structure. Int J Adv Manuf Technol 107:1551–1558

[26] Tang L, Feng X, Zhao GG, Li QL, Zhao JS, Ren L (2018) Cathode cross tank and return hole optimization design and experiment verification of electrochemical machining closed integral impeller outside flow channels. Int J Adv Manuf Technol 97(5-8):2921-2931

[27] Fujisawa T, Inaba K, Yamamoto M, Kato D (2008) Multiphysics simulation of electrochemical machining process for three-dimensional compressor blade. J Fluids Eng 130(8):081602-1-7

[28] Analytis GT (2001) Implementation and assessment of the renormalization group (RNG), quadratic and cubic non-linear eddy viscosity k-ε models in GOTHIC. Nucl. Eng Des 210:177–191

[29] Koutsourakis N, Bartzis JG, Markatos NC (2012) Evaluation of Reynolds stress, k-ε and RNG k-ε turbulence models in street canyon flows using various experimental datasets. Environ Fluid Mech 12:379–403